Time evolution and squeezing of the field amplitude in cavity QED

J. E. Reiner, W. P. Smith, and L. A. Orozco

Department of Physics and Astronomy, State University of New York, Stony Brook, New York 11794-3800

H. J. Carmichael

Department of Physics, University of Oregon, Eugene, Oregon 97403-1274

P. R. Rice

Department of Physics, Miami University, Oxford, Ohio 45056

Received December 14, 2000; revised manuscript received June 12, 2001

We present the conditional time evolution of the electromagnetic field produced by a cavity QED system in the strongly coupled regime. We obtain the conditional evolution through an intensity–amplitude correlation function that measures the time evolution of the field after the detection of a photon. A connection exists between this correlation function and the spectrum of squeezing, which permits the study of squeezed states in the time domain. We calculate the spectrum of squeezing from the master equation for the reduced density matrix using both the quantum-regression theorem and quantum trajectories. Our calculations not only show that spontaneous emission degrades the squeezing signal, they also point to the dynamical processes that cause this degradation. © 2001 Optical Society of America

OCIS codes: 270.0270, 270.6570, 270.2500.

1. INTRODUCTION

Squeezing experiments focus on the control and study of quantum fluctuations. In a squeezed state there is a redistribution of the fluctuations between the different quadratures of the electromagnetic field. This modification is measurable through the spectrum of squeezing and its comparison with that of the vacuum state. In this paper we analyze the time evolution of the quantum fluctuations of the electromagnetic field, the complementary picture of the spectral density studied in squeezing. We use a new formalism based on a third-order correlation function of the field. This intensity–amplitude correlation is a conditional measurement of the amplitude of the field because of the quantum nature of the intensity measurement.

By combining the wave and particle aspects of light, this correlation function brings a new theoretical[1] and experimental[2,3] understanding to the study of the quantum properties of squeezed light. This is because the intensity–amplitude correlation function and the spectrum of squeezing form a Fourier-transform pair when third-order moments of the field fluctuations are neglected. We can now analyze the conditional time evolution of the fluctuations that give rise to the redistribution of the noise between the two quadratures of the electromagnetic field.

Work on the spectrum of squeezing is a well established area of research.[4,5] The interaction between a single cavity mode of the electromagnetic field and several two-level atoms produces nonclassical fields that exhibit squeezing. Work on this system started with the study of optical bistability[6–10] (OB). These OB systems are treated in the limit of small noise, such that the fluctuations are only a minimal perturbation on the steady state. More recent work has focused on a regime where there is no small-size parameter and fluctuations dominate the behavior of the system.[11] This general area is cavity QED.[12] While there are experimental realizations in the microwave and optical regimes, our discussion will only consider the latter. In both systems the reversible coupling between the atoms and the cavity mode is larger than the irreversible loss of coherence from spontaneous emission or cavity decay. A number of optical studies, experimental and theoretical, have focused on the nonclassical features as observed in the intensity correlations, such as photon antibunching.[13–16] Our recent observations look, however, at the time dependence of the conditional fluctuations of the field[2] and its connection with the spectrum of squeezing.

The experiment revealed that the spectrum of squeezing degrades when the conditional fluctuation oscillates about a nonuniform background rather than the steady-state field amplitude. In order to understand this behavior we apply the time-domain formalism to the strong-coupling regime of cavity QED. To keep the discussion manageable, we only treat the case of one or two atoms fixed in space. The work follows the general philosophy[17,18] where cavity QED is analyzed without a small parameter.

The paper is organized as follows. In Section 2 we describe the intensity–amplitude correlation function and its connection to the spectrum of squeezing. Section 3

0740-3224/2001/121911-11$15.00

discusses the properties of the cavity QED system. Section 4 shows the different techniques utilized to calculate the spectrum of squeezing and the intensity–amplitude correlation function. We present our results in Section 5, the discussion of those results in Section 6, and our conclusions in Section 7.

2. INTENSITY–AMPLITUDE CORRELATION FUNCTION

Consider a general system in which a signal field is emanating from a source. Figure 1 shows the apparatus that measures the correlation between the amplitude and the intensity of this electromagnetic field. The correlation is measured by first detecting a photon in an avalanche photodiode (APD), which triggers the recording of the photocurrent output of a balanced homodyne detector[2] (BHD). This conditioned photocurrent, $\mathcal{H}(\tau)$, is averaged over N_s starts,

$$\mathcal{H}(\tau) = \frac{\langle :\hat{A}(0)\hat{B}(\tau):\rangle}{\langle \hat{A}\rangle} + \sqrt{\Gamma}\xi(\tau). \tag{1}$$

Here Γ is the BHD bandwidth and $\xi(\tau)$ is the residual shot noise from averaging the photocurrent from the BHD. $\xi(\tau)$ satisfies the following correlation function:

$$\overline{\xi(0)\xi(\tau)} = \frac{\exp(-\Gamma\tau)}{2N_s}. \tag{2}$$

The operators $\hat{A}$ (intensity measurement) and $\hat{B}$ (field measurement) depend on the fraction of light sent to the APD, r (see Fig. 1). When the signal mode $\hat{b}$ has a mean, $\langle \hat{b}\rangle = \lambda$, the operators $\hat{A}$ and $\hat{B}$ are

$$\hat{A} = 2\Upsilon r\hat{b}^\dagger\hat{b}, \tag{3}$$

$$\hat{B} = \sqrt{2\Upsilon(1-r)}\hat{Q}_\theta, \tag{4}$$

where $\hat{Q}_\theta \equiv [\hat{b}\exp(-i\theta) + \hat{b}^\dagger\exp(i\theta)]/2$ is the quadrature amplitude selected by the local-oscillator phase and 2Υ is the flux rate. Carmichael *et al.* have generalized Eqs. (3) and (4) to any source,[1] but for the purpose of this paper it is sufficient to limit the discussion to the detection scheme of Fig. 1.

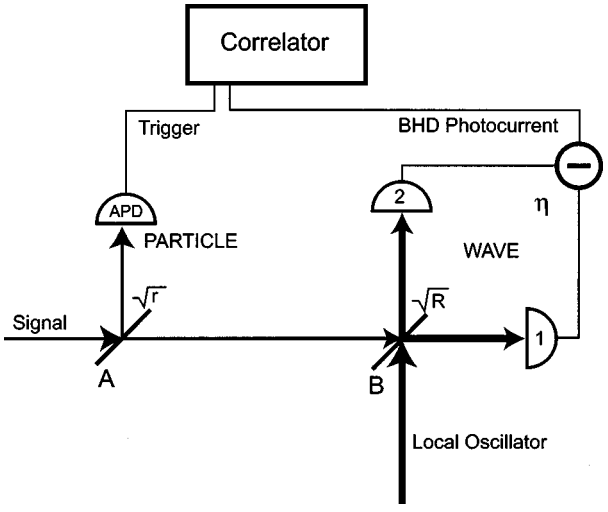

Fig. 1. Schematic of the intensity–amplitude correlator. The intensity reflectivity of beam splitters A and B is given by r and R, respectively. η is the efficiency of the balanced homodyne detector.

We derive an expression for the photocurrent in terms of the fluctuations in the signal field by writing $\hat{b} = \lambda\exp(i\theta) + \Delta\hat{b}$. In the limit of Gaussian fluctuations we may neglect the third-order moment of the field fluctuations, and the correlation function is[2]

$$\mathcal{H}(\tau) = \sqrt{8\Upsilon(1-r)}\lambda\left[1 + 2\frac{\langle :\Delta\hat{Q}_\theta(0)\Delta\hat{Q}_\theta(\tau):\rangle}{\lambda^2 + \langle\Delta\hat{b}^\dagger\Delta\hat{b}\rangle}\right] + \sqrt{\Gamma}\xi(\tau). \tag{5}$$

A normalized, conditioned-field correlation function results from normalizing this equation by the steady-state field at the BHD:

$$h_\theta(\tau) = 1 + 2\frac{\langle :\Delta\hat{Q}_\theta(0)\Delta\hat{Q}_\theta(\tau):\rangle}{\lambda^2 + \langle\Delta\hat{b}^\dagger\Delta\hat{b}\rangle} + \frac{\sqrt{\Gamma}\xi(\tau)}{\sqrt{8\Upsilon(1-r)}\lambda}. \tag{6}$$

The shot-noise contribution in Eq. (6) is determined by the number of samples averaged. To obtain a good signal-to-noise ratio for $h_\theta(\tau)$, we have to reduce the shot-noise contribution by averaging over many realizations, N_s, such that the averaged correlation, $\overline{h_\theta(\tau)}$, is

$$\overline{h_\theta(\tau)} = \lim_{N_s=\infty} h_\theta(\tau) = 1 + 2\frac{\langle :\Delta\hat{Q}_\theta(0)\Delta\hat{Q}_\theta(\tau):\rangle}{\lambda^2 + \langle\Delta\hat{b}^\dagger\Delta\hat{b}\rangle}. \tag{7}$$

Note that this average is independent of both the fraction of light, $1-r$, sent to the BHD and the quantum efficiencies of the detectors. They only enter in the remaining shot noise, which is present in the laboratory measurement.

The spectrum of squeezing is the cosine transform of the normalized correlation function,

$$S(\theta,\nu) = 4F\int_0^\infty d\tau\cos(2\pi\nu\tau)[\overline{h_\theta(\tau)} - 1]. \tag{8}$$

$F = 2\Upsilon\langle\hat{b}^\dagger\hat{b}\rangle$ is the photon flux into the correlator.

A standard squeezing measurement is performed by sending the photocurrent output from a BHD into a frequency analyzer and comparing it with the shot-noise level. This detection scheme depends on detector efficiencies and propagation errors.[19] Additionally, the system restricts the measurement of the spectrum of squeezing to only one frequency at a time. The intensity–amplitude correlator overcomes these difficulties. First, the fluctuations in time reveal the entire spectrum of squeezing up to a frequency set by the detector bandwidth. Second, the BHD efficiency only enters through the residual shot noise in Eq. (6), which can be removed by averaging over many starts.

3. CAVITY QED SYSTEM

The fluctuations in the signal beam in Fig. 1 must be squeezed by a nonlinear source. The source we consider here originates from a cavity QED system. We consider a cavity QED system that consists of a single mode of the

electromagnetic field interacting with a collection of two-level atoms (see Fig. 2). Two spherical mirrors form an optical cavity that defines the field mode. We consider only a single atom or a pair of two-level atoms optimally coupled to the mode of the cavity. Dissipation plays an important role as both the atoms and the field couple to reservoirs. An atom can spontaneously emit light into modes other than the preferred mode, and light inside the cavity can escape through the mirrors. We assume that the fractional solid angle subtended by the cavity mode is small enough that we do not have to account for corrections to the atomic-decay rates. A coherent field, injected through one of the mirrors, drives the system. The signal beam in Fig. 1 is the light that escapes from the cavity through the output mirror.

The Jaynes–Cummings Hamiltonian[20] describes the interaction of a two-level atom with a single mode of the quantized electromagnetic field,

$$\hat{H} = \hbar\omega_a\hat{\sigma}^z + \hbar\omega_c\hat{a}^\dagger\hat{a} - i\hbar g(\hat{\sigma}_+\hat{a} - \hat{a}^\dagger\hat{\sigma}_-), \qquad (9)$$

where $\hat{\sigma}_\pm$ and $\hat{\sigma}^z$ are the Pauli spin operators for raising, lowering, and inversion of the atom, and $\hat{a}^\dagger$,$\hat{a}$ are the raising and lowering operators for the field. The eigenstates for Eq. (9) reveal the entanglement between the atom and the field. The spectrum has a first excited-state doublet with states shifted by $\pm g$ from the uncoupled resonance. The dipole coupling constant, g, is given by

$$g = \left(\frac{\mu^2\omega}{2\hbar\epsilon_0 V}\right)^{1/2}, \qquad (10)$$

where μ is the transition dipole moment, $\omega_a = \omega_c = \omega$ is the transition frequency, and V is the cavity-mode volume. The field decays out of the cavity at the rate of κ, and, considering only radiative decay, the atomic inversion decays at the rate of $\gamma = 1/\tau$ (τ is the radiative lifetime of the atomic transition).

From g, γ, and κ we can construct two dimensionless numbers from the OB literature that are useful for characterizing cavity QED systems: the saturation photon number n_0 and the single-atom cooperativity C_1. They scale the influence of a photon and the influence of an atom in the system, respectively. These two numbers relate the reversible dipole coupling between a single atom and the cavity mode (g) with the irreversible coupling to the reservoirs through cavity (κ) and inversion decays (γ) by

$$C_1 = g^2/\kappa\gamma, \qquad (11)$$

$$n_0 = \gamma^2 b/g^2, \qquad (12)$$

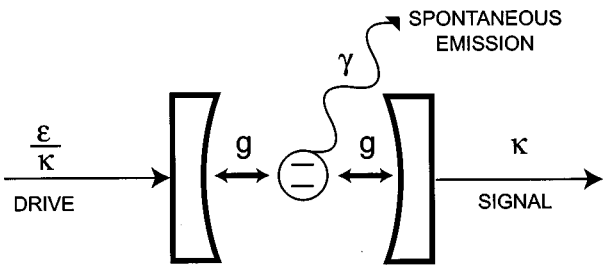

Fig. 2. Schematic of the cavity QED system.

where b is a factor that depends upon the geometry of the mode; $b = 1/8$ for a plane wave.[13]

The values of C_1 and n_0 define the different regimes of OB and cavity QED. Our analysis focuses on the strong-coupling regime of cavity QED ($n_0 < 1$, $C_1 > 1$), which implies large effects from the presence of a single photon and of a single atom in the system. Consequently, a change of one photon represents a large fluctuation in the system.

We consider only the resonant case here, with the driving field on resonance with both the atomic transition and the cavity-mode frequency. This means that we are only able to explore dynamical changes in one quadrature. A generalization to other phases requires either the driving of the system off resonance or the addition of a coherent offset similar to the one discussed in Ref. 1.

Two dimensionless fields and intensities follow from the OB literature that allow us to make contact with experiments: The intracavity field (intensity) with atoms in the cavity is given by $x \equiv \langle\hat{a}\rangle/\sqrt{n_0}$ ($X \equiv \langle\hat{a}^\dagger\hat{a}\rangle/n_0$), and the field (intensity) without atoms in the cavity is given by $y \equiv \mathcal{E}/\kappa\sqrt{n_0}$ ($Y = y^2$), where $2\mathcal{E}^2/\kappa$ is the input photon flux.

4. CALCULATIONS OF THE INTENSITY–AMPLITUDE CORRELATION FUNCTION IN CAVITY QED

We present the two different methods used to calculate the intensity–amplitude correlation function. The first is a direct calculation from the master equation and the second is a quantum-trajectory simulation.

A. Direct Calculation from the Master Equation

A master equation of the Lindblad form can be derived for the system shown in Fig. 2 by use of standard techniques.[21] This equation for the reduced density operator $\hat{\rho}$ for the case of N atoms identically coupled to a single cavity mode reads

$$\begin{aligned}\dot{\hat{\rho}} \equiv \mathcal{L}\hat{\rho} = {} & \mathcal{E}[\hat{a}^\dagger - \hat{a},\hat{\rho}] + g[\hat{a}^\dagger\hat{S}_- - \hat{a}\hat{S}_+,\hat{\rho}] \\ & + \kappa(2\hat{a}\hat{\rho}\hat{a}^\dagger - \hat{a}^\dagger\hat{a}\hat{\rho} - \hat{\rho}\hat{a}^\dagger\hat{a}) \\ & + \gamma/2\sum_{j=1}^{N}(2\hat{\sigma}^j_-\hat{\rho}\hat{\sigma}^j_+ - \hat{\sigma}^j_+\hat{\sigma}^j_-\hat{\rho} - \hat{\rho}\hat{\sigma}^j_+\hat{\sigma}^j_-),\end{aligned} \qquad (13)$$

where $\hat{S}_\pm = \Sigma_j\sigma^j_\pm$ are the collective raising and lowering operators for the atoms.

Early attempts at solving this master equation are found in the OB literature.[6,7] These approaches involved converting the master equation into a c-number Fokker–Planck equation with a large N expansion. A connection was then made to a set of Itô stochastic differential equations. This master equation could thus be solved analytically, but only for the case of small fluctuations.

Our cavity QED system operates in the strongly coupled regime where the effective number of atoms and the size of the quantum fluctuations, relative to the steady state, will not permit us to make any of the assumptions mentioned above. Instead, we numerically

solve the master equation in a manner similar to that described by Brecha *et al.*[18] We transform the master equation into frequency space and apply the quantum-regression theorem of Lax[22,23] to calculate the spectrum of squeezing directly. We check the accuracy of our results by increasing the maximum number of photons included in the basis, $n_{\max}$, until the value of the squeezing at any given frequency is accurate to three significant digits. This approach permits us to calculate the spectrum of squeezing for the cavity QED system away from the low-intensity limit and it allows us to consider the case of either one or two atoms.

B. Quantum Trajectories

Studying the intensity–amplitude correlator with quantum trajectories requires some justification. This subsection provides that justification. We begin with a review of some of the fundamental concepts behind quantum-trajectory theory. Much of the important work done in the field of quantum trajectories and stochastic Schrodinger equations can be found in the review by Plenio and Knight[24] and references therein. This presentation follows the work of Carmichael.[21]

An alternative approach to studying a master equation of the Lindblad form can be formulated with quantum-trajectory theory. To create quantum trajectories one must unravel the master equation. We are only interested in those unravelings that correspond directly to an experimental measurement. This measurement probes the system by opening channels between the system and the environment. Excitations into these channels are represented by the following superoperator:

$$S_i\hat{\rho} = \hat{k}(\hat{s}_i,\hat{s}_i^\dagger)\hat{\rho}\hat{k}^\dagger(\hat{s}_i,\hat{s}_i^\dagger), \tag{14}$$

where $\hat{k}$ is a function of the creation and annihilation operators, $\hat{s}_i^\dagger$ and $\hat{s}_i$, for the ith system operator coupled to the environment. The probability for the system to decay through one of these channels in a time dt depends on the occupation of that particular mode,

$$P_i = \mathrm{Tr}(\mathcal{S}_i\hat{\rho})\mathrm{d}t. \tag{15}$$

Quantum trajectories also provide a picture of what is happening to the system between measurements. Equation (14) describes how measurements are performed on the system. To see what happens between measurements, we subtract Eq. (14) from Eq. (13),

$$\left(\mathcal{L} - \sum_i \mathcal{S}_i\right)\hat{\rho} = \frac{1}{i\hbar}(\hat{H}_{\mathrm{sys}}\hat{\rho} - \hat{\rho}\hat{H}_{\mathrm{sys}}^\dagger). \tag{16}$$

If we assume that the system state is initially pure, then Eqs. (14) and (16) guarantee that the conditional density operator can be written in the factorized form $\rho = |\psi\rangle\langle\psi|$. Therefore Eq. (16) implies that a propagator exists for the system wave function between measurements. This propagator is a modified, nonunitary Hamiltonian with a real and imaginary part, $\hat{H}_{\mathrm{sys}} = \hat{H}_R + i\hat{H}_I$.

Below is the quantum-trajectory algorithm that propagates the system wave function forward in time.

1. Choose an initial state for the system.

2. Calculate the probability for the system to decay through each of the loss channels from Eq. (15):

$$P_i = \langle\hat{k}^\dagger(\hat{s}_i)\hat{k}(\hat{s}_i)\rangle\mathrm{d}t. \tag{17}$$

3. Associate a uniformly distributed random number between 0 and 1 with each loss channel in step 2. If the probability for the ith channel is greater than its corresponding random number, then we collapse the system wave function,

$$|\psi(t + \mathrm{d}t)\rangle = \hat{k}(\hat{s}_i)|\psi(t)\rangle. \tag{18}$$

In the unlikely event of multiple collapses, choose only one collapse with another random number.

4. If the probability for loss through each channel is less than the corresponding random numbers, then propagate the system wave function with the effective Hamiltonian from Eq. (16),

$$|\psi(t + \mathrm{d}t)\rangle = \left(1 - \frac{\hat{H}_{\mathrm{sys}}}{i\hbar}\mathrm{d}t\right)|\psi(t)\rangle. \tag{19}$$

5. Normalize the system wave function and repeat from step 2.

This is the basis for quantum trajectories. The master equation describes the evolution of the reduced density matrix. A connection is made between this density matrix and a system wave function. This wave function leads to measurements with losses through the system's decay channels. These measurements update our knowledge of the system wave function. This allows one to study how measurements performed on a system will, through conditioning, affect the system state.

In order to unravel Eq. (13) with the intensity–amplitude correlator we need to first add the BHD to the system. The BHD consists of a local oscillator that is modeled by a driven, single-mode coherent field. We write the master equation for the system plus the local-oscillator mode as

$$\begin{aligned}\dot{\hat{\rho}} = {} & \mathcal{E}[\hat{a}^\dagger - \hat{a},\hat{\rho}] + g[\hat{a}^\dagger\hat{S}_- - \hat{a}\hat{S}_+,\hat{\rho}] \\ & + \kappa(2\hat{a}\hat{\rho}\hat{a}^\dagger - \hat{a}^\dagger\hat{a}\hat{\rho} - \hat{\rho}\hat{a}^\dagger\hat{a}) \\ & + \kappa_{LO}(2\hat{c}\hat{\rho}\hat{c}^\dagger - \hat{c}^\dagger\hat{c}\hat{\rho} - \hat{\rho}\hat{c}^\dagger\hat{c}) + \kappa_{LO}\chi[\hat{c}^\dagger - \hat{c},\hat{\rho}] \\ & + \gamma/2\sum_{j=1}^{N}(2\hat{\sigma}_-^j\hat{\rho}\hat{\sigma}_+^j - \hat{\sigma}_+^j\hat{\sigma}_-^j\hat{\rho} - \hat{\rho}\hat{\sigma}_+^j\hat{\sigma}_-^j),\end{aligned} \tag{20}$$

where $\hat{c}^\dagger$ and $\hat{c}$ represent the raising and lowering operators for the local-oscillator mode. The coherent field occupies a mode whose strength we denote by χ. Under a BHD scheme the beam splitter combines the signal and local-oscillator fields equally ($R = 1/2$), as in Fig. 1, to give the following total measured fields at photodetectors 1 and 2,

$$\hat{\mathcal{E}}_{\mathrm{BHD}^{1,2}} = \pm i\sqrt{\kappa_{\mathrm{LO}}}\hat{c} + \sqrt{\kappa(1-r)}\hat{a}, \tag{21}$$

and the measured field at the photon-counting detector gives

$$\hat{\mathcal{E}}_{\mathrm{count}} = \sqrt{2\kappa r}\hat{a}. \tag{22}$$

We assume that the signal mode does not affect the local-oscillator mode. This implies that the density ma-

trix separates into a piece that corresponds to the cavity QED system and a piece that corresponds to the local oscillator,

$$\hat{\rho} = \hat{\rho}_s|\chi\rangle\langle\chi|. \tag{23}$$

We define the local-oscillator flux in terms of the strength of the local-oscillator mode and its cavity decay rate,

$$f = \kappa_{\mathrm{LO}}|\chi|^2. \tag{24}$$

From Eq. (14) we construct the master-equation terms that correspond to Eqs. (21) and (22) and spontaneous emissions:

$$\mathcal{S}_{\mathrm{BHD}^{1,2}}\hat{\rho}_s = [\pm\sqrt{f}\exp(i\theta) + \sqrt{2\kappa(1-r)}\hat{a}] \times \hat{\rho}_s[\pm\sqrt{f}\exp(-i\theta) + \sqrt{2\kappa(1-r)}\hat{a}^\dagger] \tag{25}$$

$$\mathcal{S}_{\mathrm{count}}\hat{\rho}_s = 2\kappa r\hat{a}\hat{\rho}_s\hat{a}^\dagger, \tag{26}$$

$$\mathcal{S}_{\mathrm{spont}}\hat{\rho}_s = \gamma\hat{\sigma}_-\hat{\rho}_s\hat{\sigma}_+. \tag{27}$$

After subtracting Eqs. (25)–(27) from Eq. (20), we arrive at an expression that corresponds to Eq. (16),

$$\begin{aligned}(\mathcal{L} - \mathcal{S}_{\mathrm{BHD}^{1,2}} - \mathcal{S}_{\mathrm{count}} - \mathcal{S}_{\mathrm{spont}})\hat{\rho}_s &= \mathcal{E}[\hat{a}^\dagger - \hat{a}, \hat{\rho}_s] + g[\hat{a}^\dagger\hat{S}_- - \hat{a}\hat{S}_+, \hat{\rho}_s] \\ &\quad - \kappa(\hat{a}^\dagger\hat{a}\hat{\rho}_s + \hat{\rho}_s\hat{a}^\dagger\hat{a}) \\ &\quad - \gamma/2\sum_{j=1}^{N}(\hat{\sigma}^j_+\hat{\sigma}^j_-\hat{\rho}_s + \hat{\rho}_s\hat{\sigma}^j_+\hat{\sigma}^j_-) - f\hat{\rho}_s.\end{aligned} \tag{28}$$

Equation (28) provides a modified Hamiltonian that propagates the system's wave function between measurements. Equations (25) and (26) govern how "clicks" at the BHD and APD disrupt that evolution.

There are two types of detections, not including spontaneous emissions, that occur under the conditional BHD measurement. The first comes from Eq. (26), which corresponds to detections at the APD. According to Eq. (15), these collapses occur with a probability of $2\kappa r\langle\hat{a}^\dagger\hat{a}\rangle\mathrm{d}t$, and they produce a significant change in the wave function as is evident from Eq. (18).

The second type of collapse corresponds to the "clicks" at the BHD. The strength of the local oscillator tells us that there are many BHD clicks within a time interval set by κ^{-1}. Equation (18) shows that the effect of each of these clicks on the system wave function is almost negligible. This implies that a straightforward trajectory simulation with the algorithm described above in Eqs. (17)–(19) will not provide an efficient method for modeling the intensity–amplitude correlator. Instead, we may associate a photocurrent with the detections registered by the BHD. The superposition of the cavity field with the local-oscillator field in Eq. (21) implies that the BHD photocurrent and the system wave-function evolution are not independent. With the principles outlined in Sections 8.4, 9.2, and 9.4 of Ref. 21 we combine Eqs. (25)–(28) to simultaneously calculate this photocurrent from the BHD setup and then evolve a corresponding stochastic Schrödinger equation forward in time. This analysis leads to the following expressions for the difference in photocurrents between photodetectors 1 and 2 in Fig. 1 and also wave-function propagation between photodetections at the APD and spontaneous emissions out the sides of the cavity:

$$\mathrm{d}i = -\Gamma[i\,\mathrm{d}t - \sqrt{8\kappa(1-r)}\langle\hat{a}_\theta\rangle_c\mathrm{d}t + \mathrm{d}W_t], \tag{29}$$

$$d|\bar{\psi}\rangle_c = \left\{\frac{H_{\mathrm{sys}}}{i\hbar}\,\mathrm{d}t + \sqrt{2\kappa(1-r)}\hat{a}\exp(-i\theta) \times [\sqrt{8\kappa(1-r)}\langle\hat{a}_\theta\rangle_c\mathrm{d}t + \mathrm{d}W_t]\right\}|\bar{\psi}\rangle_c, \tag{30}$$

where Γ is the BHD bandwidth and $\mathrm{d}W_t$ is the same Wiener noise increment in both equations.

This BHD difference current $i(t)$, along with a set of start times $\{t_j\}$, form a stochastic measurement record. We simulate Eqs. (29) and (30) on a computer. By sampling an ongoing realization of $i(t)$ for many "start" times (APD detections realized concurrently), we may calculate the following averaged photocurrent:

$$\mathcal{I}(\tau) = \frac{1}{N_s}\sum_{j=1}^{N_s} i(t_j + \tau). \tag{31}$$

By averaging over many starts, we remove the shot-noise contribution from Eq. (29). What remains is an equation that relates the photocurrent with the conditioned-field evolution, $\langle\hat{a}_\theta\rangle_c$. The averaged photocurrent gives the normalized conditioned field that is the intensity–amplitude correlation function.[1] In the limit of large bandwidth we obtain

$$h_\theta(\tau) = \frac{\mathcal{I}(\tau)}{\langle\hat{a}\rangle\sqrt{8\kappa(1-r)}}. \tag{32}$$

The dual nature of the measurement process provides one of the many strengths of the conditional-field measurement. It allows the use of quantum-trajectory theory to unravel the master equation in two distinct ways. A numerical simulation of Eqs. (29) and (30) reproduces the experimental results for the averaged photocurrent. We can understand some of the mechanisms that lead to this averaged result by simulating the algorithm described in Eqs. (17)–(19) and replacing Eq. (19) with Eq. (30). Setting $r \approx 1$ reduces the conditional homodyne simulation to a cleaner photocounting simulation. This leads to an understanding of the dynamical processes that create the spectrum of squeezing.

5. RESULTS

The simplest parameter to change during the course of the experiment is the strength of the driving field. This motivates our study of the effect of driving intensity on the spectrum of squeezing. The strength of the driving field is parameterized in terms of the saturation photon number, n_0. Therefore weak fields imply $X \ll 1$, for intermediate fields $X \approx 1$, and strong fields correspond to $X \gg 1$. We begin by reporting the results of a low-intensity calculation with both the quantum trajectories

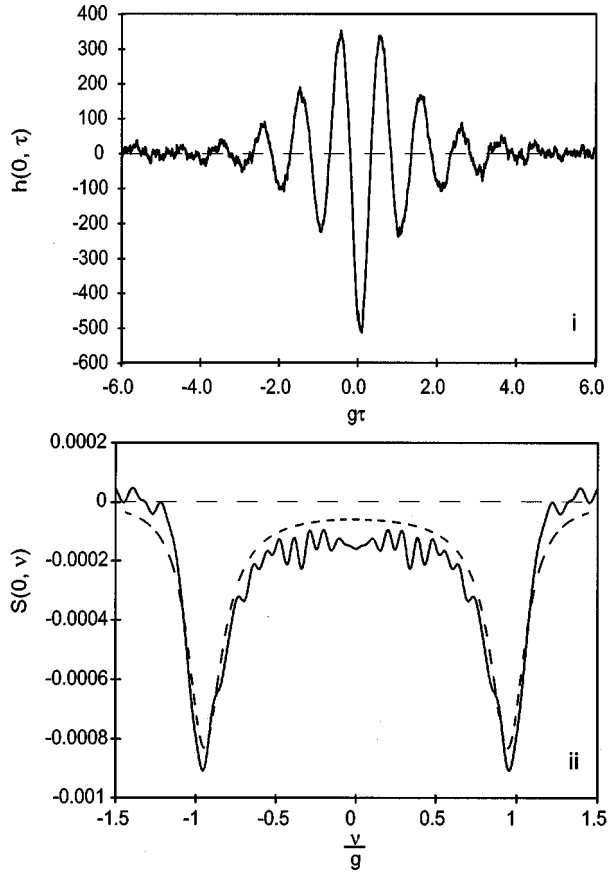

Fig. 3. (i) Intensity–amplitude correlation $h(0°, \tau)$ for very low intensity excitation calculated from the quantum-trajectory implementation of the conditioned homodyne photocurrent. The following parameters were used: $(g, \kappa, \gamma, \Gamma)/(2/\pi) = (38.0, 8.7, 3.0, 100)$ MHz, $X = 2.99 \times 10^{-4}$, $r = 0.5$, and $N_{\text{starts}} = 55\,000$. (ii) Spectrum of squeezing calculated from the cosine Fourier transform of $h(0°, \tau)$. The dashed curve is the spectrum of squeezing calculated directly from the master equation with the quantum-regression theorem.

and the direct calculation from the master equation. We then increase the intensity of the driving field and also the number of atoms in the cavity from one to two. This degrades the spectrum of squeezing in a way that we hope to understand through the study of quantum trajectories.

A. Low-Intensity Results for $h(0°, \tau)$ and $S(0°, \nu)$

Figure 3 shows the equivalence of the third-order correlation function $h(0°, \tau)$ (i) and the spectrum of squeezing (ii) for a strongly coupled cavity QED system. The dashed curve in Fig. 3ii is the spectrum of squeezing calculated directly from the quantum-regression theorem. The solid curve is the Fourier transform [see Eq. (8)] of Fig. 3i that comes from averaging the photocurrent from a quantum-trajectory simulation over 55 000 "starts." Both approaches show the damped Rabi oscillations that precede and follow a photodetection. In the weak-field excitation limit, Rice and Carmichael[25] derived an analytical expression for the spectrum of squeezing that agrees with these results.

One may notice an apparent discrepancy between the size of the fluctuations in Fig. 3i, which are quite large with respect to the steady state, and the degree of squeezing shown in Fig. 3ii. In the weak-field limit the cavity field spends a majority of its time in the steady state. This means that fluctuations may be very large, but the time between them is also very long. These two competing effects lead to very small degrees of squeezing. In this paper we are more interested in the dynamics of the cavity field rather than in achieving large degrees of squeezing.

Detecting a photon in the APD collapses the state of the cavity field. The oscillations in the field after a detection show the collapsed state oscillating back toward the steady state. In the Gaussian noise approximation the time symmetry of the measured correlation function, Eq. (6), guarantees the oscillation before the detection.

B. From One Atom to Two Atoms at Intermediate Intensity

It has not been possible to obtain analytical expressions for the spectrum of squeezing in the case of intermediate driving fields. In this regime one cannot linearize the system fluctuations about the steady-state field as was done in the strong-field case.[26] It is also impossible to perform a small-parameter expansion in the driving field as was done in the weak-field case.[17] We are instead forced to rely on numerical calculations of the type described in Subsection 4.A to give us insight into the system's spectrum of squeezing. This approach has its limitations.

The spectra of squeezing for increased excitation in the case of one and two atoms have distinct quantitative differences. Figure 4 shows one such spectrum calculated for a driving field of $\mathcal{E}/\kappa = 1.50$ and one atom. Figure 5 shows the result for two atoms with $\mathcal{E}/\kappa = 0.975$. We calculated both plots directly from the master equation as was described in Subsection 4.A. We used the same decay parameters for both plots but different atom field couplings, g, in order to keep the Rabi frequency, $g\sqrt{N}$, the same.

We would like to understand the degradation of the spectrum of squeezing by incoherent processes that occur at zero frequency. This is done by studying the full width

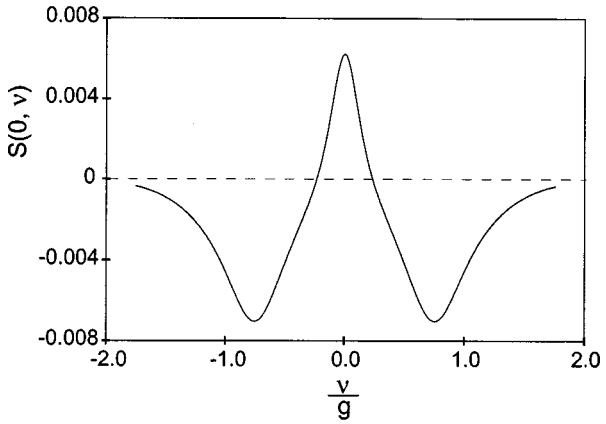

Fig. 4. Spectrum of squeezing calculated directly from the master equation with the quantum-regression theorem for $N = 1$ and high intensity. $X = 104.0$, $(g, \kappa, \gamma)/(2\pi) = (38.0, 8.7, 3.0)$ MHz.

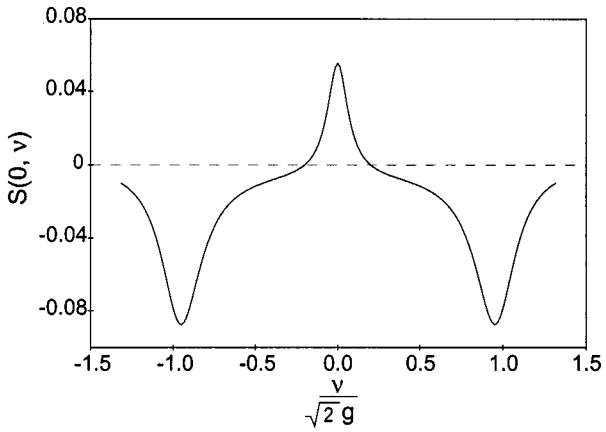

Fig. 5. Spectrum of squeezing calculated directly from the master equation with the quantum-regression theorem for $N = 2$ and intermediate intensity. $X = 1.36$, $(g, \kappa, \gamma)/(2\pi) = (38.0/\sqrt{2}, 8.7, 3.0)$ MHz.

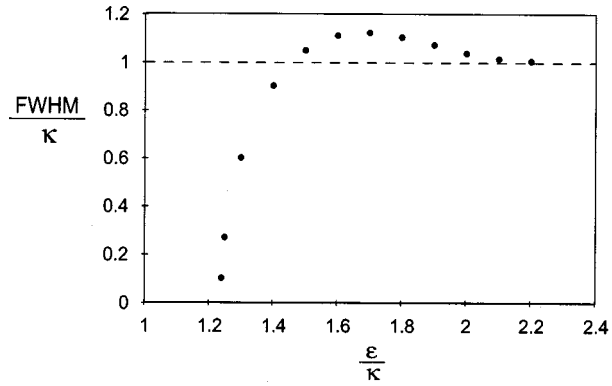

Fig. 6. Dependence of the width of the peak at zero frequency in the squeezing spectrum as a function of the input driving strength for $N = 1$. The following parameters were used: $(g, \kappa, \gamma)/2\pi = (38.0, 8.7, 3.0)$ MHz. The FWHM has been normalized by the cavity decay rate, κ.

at half-maximum (FWHM) of the peak at zero frequency for both the one and the two atom cases.

The width and the shape of the peaks centered at zero frequency are very different between the one- and two-atom spectra of squeezing. For the case of the single atom it is clear from Fig. 6 that the cavity-decay rate dominates the degradation. In order to see a peak at zero frequency one must drive the one-atom system much harder than the two-atom system; we note that the intracavity intensity, normalized by the saturation photon number, is nearly 100 times greater for the one atom case. This is understood because with a strong enough driving field the single atom will be saturated. At this point most of the photons that enter the cavity will bounce between the two mirrors without ever interacting with this single atom. This leads to less squeezing and a peak in the zero-quadrature spectra at zero frequency with a width that is dominated by the cavity lifetime.

Figure 7 shows a plot of the FWHM for different driving fields in the two-atom system. Here spontaneous emission plays a more influential role. This is not surprising because the coupling to the environment leads to a degradation of the squeezing signal, and these incoherent processes appear at zero frequency in the interaction picture. The quantitative results may vary for system parameters that differ from our experiment such as $\kappa < \gamma$, but the parameters that we use will allow us to see how spontaneous emission, which becomes more prominent as the number of atoms in the cavity increases, can lead to the degradation of the spectrum of squeezing. The question we hope to answer with quantum trajectories is the following: What is the mechanism by which spontaneous emission gives rise to this degradation in the squeezing signal?

C. High Intensity

A large positive peak in the spectrum of squeezing appears at zero frequency when we increase the strength of the driving field to the case when there is about one-tenth of a photon in the cavity and two atoms interacting with the mode. Negative peaks appear at a frequency less than that of the coherent coupling, g, between the atoms and the field. Figure 8i shows the result of directly solving the master equation with the quantum-regression theorem.

The connection between the spectrum of squeezing and the time-domain fluctuations shows that on average the conditioned field undergoes an exponential damping that is not present for the weaker driving fields (see Fig. 8ii). The careful reader may think there is a slight problem in saying that the connection between the spectrum of squeezing and the third-order correlation function still holds in these stronger fields. We will show, from the results of a quantum-trajectory simulation in Subsection 6.B, that the qualitative behavior of the fluctuations remains the same. Therefore the third-order correlation function provides a legitimate method for studying the spectrum of squeezing beyond the weak-field approximation.

We can get a preliminary understanding of the strong-field spectrum of squeezing from the OB work of Reid and Walls.[26] They showed that in the optically bistable re-

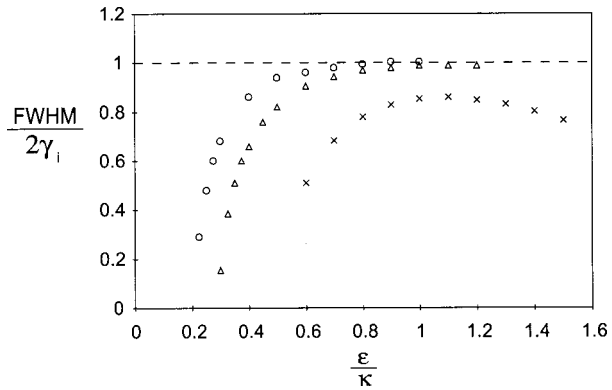

Fig. 7. Dependence of the width of the peak at zero frequency in the squeezing spectrum for three different spontaneous-emission rates as a function of the input driving strength for $N = 2$ and the following parameters: $(g, \kappa, \gamma_1, \gamma_2, \gamma_3)/2\pi = (38/\sqrt{2}, 8.7, 3.0, 1.0, 0.5)$ MHz. The FWHM for each plot has been normalized by its respective spontaneous-emission rate, γ_i. The circles are for $\gamma/2\pi = 0.5$ MHz, the triangles are for $\gamma/2\pi = 1.0$ MHz, and the x's are for $\gamma/2\pi = 3.0$ MHz. Notice the difference in driving strengths, ϵ/κ, between this figure and Fig. 6.

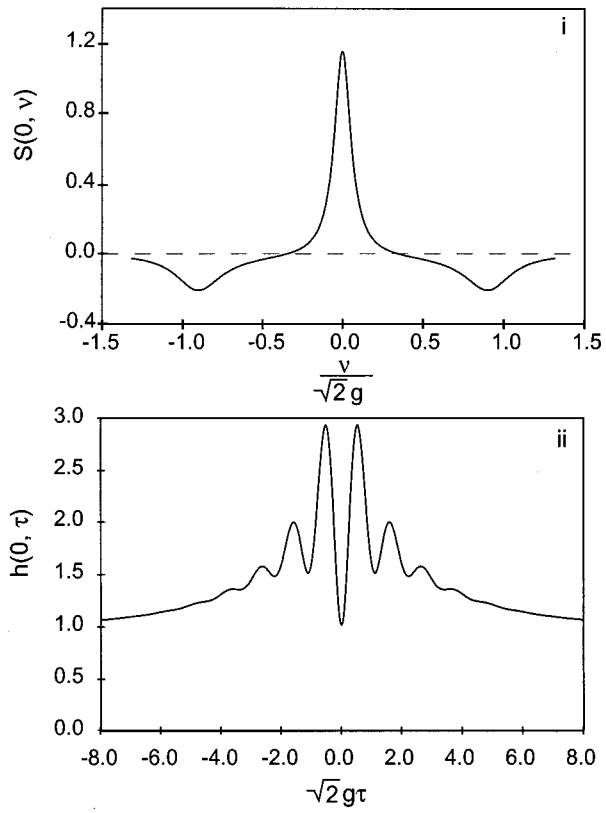

Fig. 8. (i) Spectrum of squeezing and (ii) its inverse Fourier transform for a two-atom system under a stronger driving field. This figure shows the influence of the peak at zero frequency on the fluctuations in the time domain. $X = 18.1$ and $(g, \kappa, \gamma)/(2\pi) = (38.0/\sqrt{2}, 8.7, 3.0)$ MHz.

gime of a strongly driven, on-resonance cavity, the spectrum of squeezing is a Lorentzian centered at zero frequency. We understand that this peak comes from the coupling of the cavity mode to its environment, but until the recent experiments of Foster *et al.*,[2] we have had no motivation to understand the origin of this peak in the time domain.

6. DISCUSSION

We have analyzed some of the many trajectories that go into making up the third-order correlation functions shown in Section 5 by setting $r \approx 1$ in Eq. (30). We first begin by reviewing some results in the weak-field regime, and then we consider the more interesting regime of stronger driving intensities.

A. Weak-Field Trajectories

Figure 9 shows examples of the conditional-field evolution calculated with quantum-trajectory simulations. Figure 9i shows the evolution of the field following the detection of a photon escaping through the cavity mode, and Fig. 9ii shows the field evolution following the spontaneous emission of a photon out the side of the cavity. We used the following realistic parameters from the work of Foster *et al.*[2,3]: $(g, \kappa, \gamma)/2\pi = (38.0, 8.7, 3.0)$ MHz. This means that the system is in the strong-coupling regime for one and two atoms.

The basic dynamical mechanism that describes these two results can be traced back to the change of the state $|\psi\rangle$ following a collapse operation of the type found in Eq. (18). We now consider the reduction of the equilibrium state of the cavity QED system on the occasion of a triggering photon detection (see Fig. 1). Defining $\hat{A}_\theta \equiv [\hat{a}\exp(-i\theta) + \hat{a}^\dagger\exp(i\theta)]/2$, where $\hat{a}$ is the annihilation operator for the cavity field and θ is the BHD phase, we consider the quadrature amplitude, $\hat{A}_{0^\circ}$, in phase with the steady state of the field $\lambda \equiv \langle\hat{a}\rangle$. For weak excitation, and assuming fixed atomic positions $\{\mathbf{r}_j\}$, to second order in λ the equilibrium state is the pure state[17,18]

$$|\psi_{SS}\rangle = [|0\rangle + \lambda|1\rangle + (\lambda^2/\sqrt{2})\alpha\beta|2\rangle + \cdots]|G\rangle + [\phi|0\rangle + \lambda\phi\beta|1\rangle + \cdots]|E\rangle + \cdots, \quad (33)$$

where $|G\rangle$ is the one- or two-atom ground state and $|E\rangle$ is for one atom in the excited state with all others in the ground state. We assume that all the atoms are coupled to the cavity mode with the same strength, g. The explicit form for ϕ, α, and β follow from solving the master equation in the steady state.[17] They are

$$\phi = -\frac{2\sqrt{N}g}{\gamma}\lambda, \quad (34)$$

$$\alpha = 1 - 2C_1', \quad (35)$$

$$\beta = \frac{1 + 2C}{1 + 2C - 2C_1'}, \quad (36)$$

where $C \equiv NC_1$ and $C_1' \equiv C_1/(1 + \gamma/2\kappa)$.

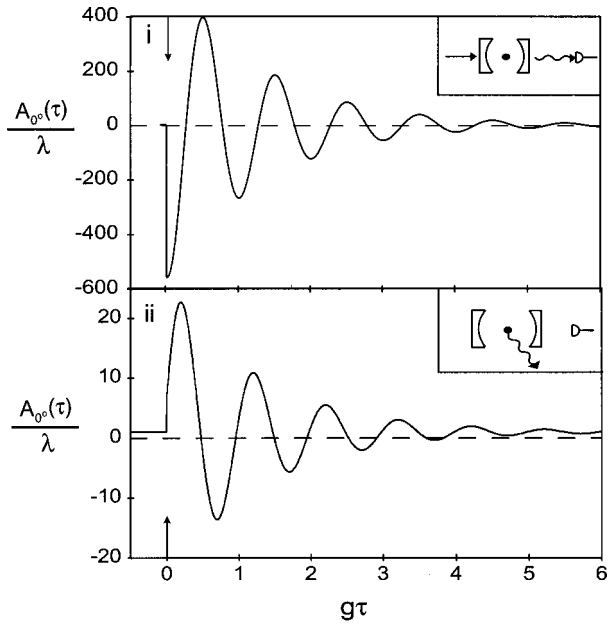

Fig. 9. Regression of a cavity QED system back to steady state; $N = 1$, low intensity (i) after the detection of a photon escaping out of the cavity mode and (ii) after the escape of a photon through spontaneous emission. The inset shows the sequence of events in terms of the cavity QED system and the detector. The parameters used are the same as in Fig. 3.

After detecting the escaping photon, the conditional state is initially the reduced state $\hat{a}|\psi\rangle/\lambda$, which then relaxes back to equilibrium. The reduction and regression is traced by[17,18]

$$|\psi\rangle \rightarrow \{|0\rangle + \lambda[1 + \zeta f(\tau)]|1\rangle + \cdots\}|G\rangle + \cdots, \quad (37)$$

where

$$\zeta = -\frac{4C_1'C}{1 + 2C - 2C_1'}, \quad (38)$$

$$f(\tau) = \exp[-(\kappa + \gamma/2)\tau/2](\cos\Omega\tau - \Phi\sin\Omega\tau), \quad (39)$$

$$\Omega = \sqrt{Ng^2 - \frac{1}{4}(\kappa - \gamma/2)^2}, \quad (40)$$

$$\Phi = -\frac{2\kappa + \gamma}{4\Omega}. \quad (41)$$

Thus the quadrature amplitude expectation makes the transient excursion $\langle\hat{A}_{0^\circ}\rangle \rightarrow \lambda[1 + \zeta f(\tau)]$ away from its equilibrium value $\langle\hat{A}_{0^\circ}\rangle = \lambda$.

In contrast, an undetected spontaneous emission produces the reduced state $\hat{\sigma}^-|\psi\rangle/\lambda$, which sets up a completely different evolution as shown in Fig. 9ii. The reduction and regression in this case is again traced by Eq. (37) with the following replacements:

$$\zeta = \frac{2C_1'}{1 + 2C - 2C_1'}, \quad (42)$$

$$\Phi = \frac{2\kappa - \gamma}{4\Omega} + \frac{2Ng^2\left(\frac{q\beta}{\sqrt{2}} - 1\right)}{\gamma\Omega(\beta - 1)}, \quad (43)$$

with $q = \sqrt{1 - 1/N}$.

These two distinct behaviors correspond fairly loosely to the regression to equilibrium observed in the step excitation in the field, Fig. 9i, and a step excitation in the atomic polarization, Fig. 9ii. Note the phase shift between the two responses. The steady-state wave function determines the size of the steps:

$$\frac{\langle\hat{A}_{0^\circ(\text{cavity})}\rangle}{\langle\hat{A}_{0^\circ(\text{steadystate})}\rangle} = \alpha\beta, \quad (44)$$

$$\frac{\langle\hat{A}_{0^\circ(\text{spontaneous})}\rangle}{\langle\hat{A}_{0^\circ(\text{steadystate})}\rangle} = \beta. \quad (45)$$

We see from Eq. (36) that β is a number greater than zero. The field will always remain positive when an atom spontaneously emits. As long as $g > \sqrt{\gamma(\kappa + \gamma/2)/2}$, then through α [Eq. (35)], the field will change sign when a photon escapes through the cavity mode.

The parameters used to create the plots in Fig. 9 are the same as those used in Fig. 3. Except for the residual shot noise in Fig. 3i, these two plots are in agreement with each other for $\tau > 0$.

B. High Field Trajectories

The weak-field calculations of Subsection 6.A make it clear that in the strong-coupling regime a cavity emission will always produce a negative shift in the field. In order for us to observe fields of the type in Fig. 8ii and spectra of squeezing of the type in Figs. 4, 5, and 8i, we must find a mechanism that causes the expectation of the cavity field to jump positive after a cavity emission.

It follows from Eq. (33) that the ratio of the probability for a spontaneous emission to the probability for a cavity emission from steady state is

$$\frac{P_{\text{spont}}}{P_{\text{cavity}}} = 2NC_1. \quad (46)$$

This implies that in the strong-coupling regime it is more likely for an atom to spontaneously emit out the sides of the cavity than for the cavity to emit a photon out through the exit mirror. Since we only begin a conditioned-field measurement after a cavity-mode emission, we should consider what happens in the likely event that a cavity photon follows a spontaneous emission.

Quantum trajectories allow one to follow the dynamics of the system under higher excitation. Figure 10 shows representative trajectories calculated from Eq. (30) when we have two atoms in the cavity and $r \approx 1$. The complete trajectory is a series of these excursions from the steady state well separated in time and a returning to the steady state as shown. In Fig. 10i the evolution starts with a spontaneous emission (A) out the side of the cavity, followed at (B) by a photon escaping through the cavity

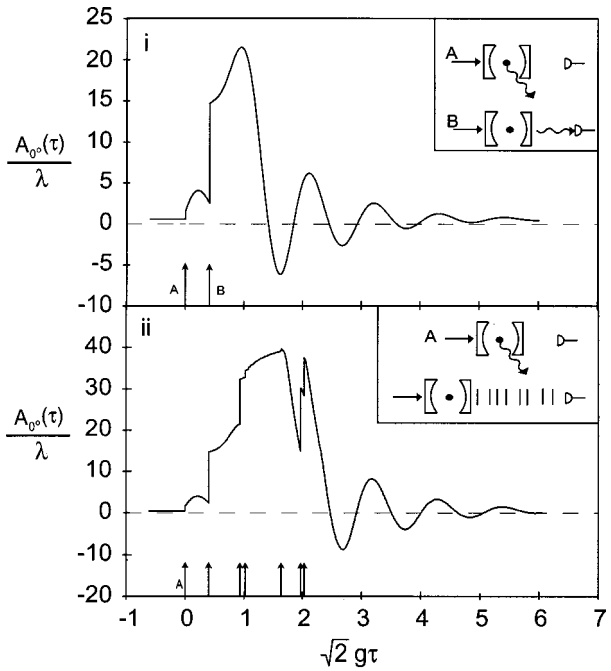

Fig. 10. Quantum-trajectory simulation that shows the time evolution of the field back to steady state after the detection of a photon. (i) A spontaneous-emission event followed by a cavity emission that starts the averaging process. (ii) A spontaneous-emission event followed by many cavity-emission events. The inset shows the sequence of events in terms of the cavity QED system and the detector. Both figures were prepared with the following parameters: $N = 2$, $X = 18.1$, and $(g, \kappa, \gamma)/(2\pi) = (38.0/\sqrt{2}, 8.7, 3.0)$ MHz.

mode that gets registered by the APD detector. Note how the field jumps positive and changes curvature with the escaping cavity photon. This is exactly the type of process that gives rise to the incoherent peak in the spectrum of squeezing because the average value of the conditioned field is much larger that the steady-state field.

We offer the following qualitative explanation of these types of events. The driving field (ϵ/κ), atom–field coupling (g), and decay rates (κ, γ) are such that the system is in a regime where the cavity field is bunched. If we have a spontaneous-emission event when the system has few excitations, we return to the steady-state value as in Fig. 3i. If the spontaneous-emission event happens while in the bunched regime, followed by a cavity emission, then there are probably more excitations in the system. With one of the atoms removed from the system following the spontaneous emission, the probability for this energy to be in the cavity mode is increased. If we detect a cavity photon soon after the spontaneous emission, then we are probably in a regime where the intracavity field undergoes a large amplitude fluctuation, and the value of the cavity field is higher than the steady-state value. This causes an upward jump in the expectation of the field. This is similar to the upward jump in the conditioned field of an optical parametric oscillator operated well below threshold.[21] In that system the conditioned steady state is small, since the system is most likely in the ground state, with a small probability of having a pair of photons in the cavity. When a photon emerges from the cavity, one photon remains, and the conditioned average field rises. It is also clear that these types of events increase linearly with the number of atoms in the cavity, since the ratio of spontaneous-emission events to cavity-loss events is $2NC_1$.

If we drive the same system much harder, the time evolution of the conditional field shows multiple jumps, some from spontaneous emission and some from escapes through the mode. The dynamics get very complicated, and we show an example in Fig. 10ii for illustration, but the general trend remains, that the average value of the field is much larger than the steady state in such cases.

Figure 10 demonstrates the power of studying the single trajectories and also provides the major result of this paper. We see that the field will have a noise background arising from the mean cavity field, on top of other quantum fluctuations, when one has a spontaneous-emission event out the side of the cavity. This is usually followed by a series of cavity emissions. This effect depends strongly on the number of atoms in the system and also on the strength of the driving field. This cannot be seen from a direct numerical solution of the master equation, but now, thanks to the conditioned-field unraveling of the master equation, we begin to see exactly how these squeezing spectra are degraded by the incoherent process of spontaneous emission.

The entire trajectory is a collection of events well separated in time of the type in Figs. 10i and 10ii. If we average over many random realizations of these different events with an initial cavity emission setting the trigger at $t = 0$, then we recover the averaged conditioned-field evolution. Figure 11 shows such an average field that after symmetrization and upon taking the Fourier transform leads to a spectrum that resembles the experimental observations qualitatively. This also shows a similar behavior as the oscillation from Fig. 4ii, and therefore a legitimate connection can still be made between the correlation function of Eq. (6) and the spectrum of squeezing slightly beyond the weak-field regime.

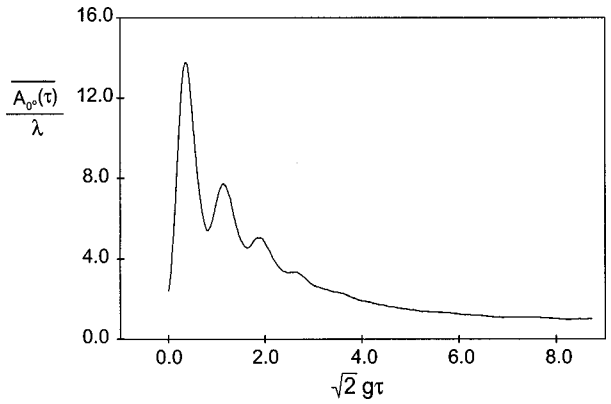

Fig. 11. Conditioned-field evolution calculated from 5000 realizations of a photon counting, quantum trajectory, simulation for $N = 2$, and high intensity. $X = 18.1$ and $(g, \kappa, \gamma)/(2\pi) = (38.0/\sqrt{2}, 8.7, 3.0)$ MHz.

C. Time Symmetry

One result that we have only briefly mentioned is the fact that Fig. 3i is symmetric with respect to $\tau = 0$, while the single events presented in Figs. 9 and 10 show a clear time asymmetry. This symmetry is recovered as a result of the BHD back action. The back action comes about because of the quantum superposition of both the local oscillator and the cavity signal field [see Eq. (21)]. It is not correct to think of these two fields as separable, a classical notion, but that each time a local-oscillator photon is detected, it also effects the evolution of the cavity field. This implies that the conditional system state at time t is correlated with the shot noise that has appeared over the recent past. Thus through the "start" clicks (particle aspect) we postselect a subensemble of the shot noise that has in effect been filtered through the system's dynamical-response function (Hamiltonian evolution).

Quantum trajectories tend to reveal precisely those physical attributes they are trying to measure. By adding the homodyne detector we attempt to measure the fluctuations in the field amplitude, and when we do this these fluctuations appear in the averaged photocurrent before the arrival of a triggering photon.

D. Future Work

By stating the problem in the time domain, we open the possibility to apply quantum-feedback theory[27,28] in order to conditionally stabilize the atom–cavity system evolution against decoherence from the environment. This stabilization will not be optimal since the information obtained is limited to the quasi mode leaking out of the cavity, and any spontaneous-emission event will be missed in the feedback loop. This calls for operating the cavity QED system in the low-intensity regime to minimize

spontaneous emission. We are currently investigating the theoretical and experimental requirements to develop such a program.

7. CONCLUSIONS

The conditional evolution of the field of a cavity QED system in the strong-coupling regime shows nonclassical behavior. This is a purely quantum-mechanical effect, and it reflects the intrinsic dynamics triggered by the collapse of the wave function after the detection (conditioning) of a photon.

Looking at the time evolution of the conditional state as it regresses back to steady state, we find that its behavior is far from random. When uninterrupted by other events, it follows a dynamic path that shows the coupling between the atom and the cavity and the significant excursion away from equilibrium brought back by a single quantum measurement. The spectrum of squeezing registers exactly the same behavior, but without the time and phase information critical to understanding the dynamics of the measurement process.

As we implement the measuring device used in the laboratory, we require an averaging process to observe the conditional evolution of the electromagnetic field. That evolution is nonclassical as shown by the squeezing. The homodyne measurement introduces back action into the system that then provides the foundation for the time-symmetric intensity–amplitude correlation function in the limit of weak driving fields.

Other avenues for the interruption of the evolution back to steady state, such as spontaneous emission, modify the correlation function, decreasing its nonclassicality. This degradation has been studied as a function of increasing system excitation. Quantum-trajectory theory demonstrates that the more likely spontaneous-emission events can trigger a burst of cavity photons that will cause the averaged conditioned field to oscillate around a nonuniform background.

The intensity–amplitude correlation function opens the door to further the study of quantum optical systems in the time domain that are necessary in order to understand better the possible realizations of quantum-feedback systems.

ACKNOWLEDGMENTS

Work was supported by the National Science Foundation.

REFERENCES

1. H. J. Carmichael, H. M. Castro-Beltran, G. T. Foster, and L. A. Orozco, "Giant violations of classical inequalities through conditional homodyne detection of the quadrature amplitudes of light," Phys. Rev. Lett. **85**, 1855–1858 (2000).
2. G. T. Foster, L. A. Orozco, H. M. Castro-Beltran, and H. J. Carmichael, "Quantum state reduction and conditional time evolution of wave-particle correlations in cavity QED," Phys. Rev. Lett. **85**, 3149–3152 (2000).
3. G. T. Foster, "Correlation measurements as a probe of fluctuations and dynamics of optical fields," Ph.D. dissertation (State University of New York, Stony Brook, 1999).
4. H. J. Kimble and D. F. Walls, eds., "Squeezed states of the electromagnetic field feature," J. Opt. Soc. Am. B **4**, 1450–1741 (1987).
5. R. Loudon and P. L. Knight, eds., "Squeezed light feature," J. Mod. Opt. **34**, 709–1020 (1987).
6. L. A. Lugiato, "Theory of optical bistability" in *Progress in Optics*, E. Wolf, ed. (North-Holland, Amsterdam, 1984), Vol. 21, pp. 69–216.
7. M. D. Reid and D. F. Walls, "Quantum theory of nondegenerate four-wave mixing," Phys. Rev. A **34**, 4929–4955 (1986).
8. M. G. Raizen, L. A. Orozco, M. Xiao, T. L. Boyd, and H. J. Kimble, "Squeezed-state generation by the normal modes of a coupled system," Phys. Rev. Lett. **59**, 198–201 (1987).
9. L. A. Orozco, M. G. Raizen, Min Xiao, R. J. Brecha, and H. J. Kimble, "Squeezed-state generation in optical bistability," J. Opt. Soc. Am. B **4**, 1490–1500 (1987).
10. D. M. Hope, H. A. Bachor, P. J. Mamson, D. E. McClelland, and P. T. H. Fisk, "Observation of quadrature squeezing in a cavity–atom system," Phys. Rev. A **46**, R1181–R1184 (1992).
11. H. J. Carmichael, "Photon antibunching and squeezing for a single atom in a resonant cavity," Phys. Rev. Lett. **55**, 2790–2793 (1985).
12. P. R. Berman, ed., *Cavity Quantum Electrodynamics*, in Advances in Atomic Molecular and Optical Physics (Academic, San Diego, 1994), Supplement 2.
13. G. Rempe, R. J. Thompson, R. J. Brecha, W. D. Lee, and H. J. Kimble, "Optical bistability and photon statistics in cavity quantum electrodynamics," Phys. Rev. Lett. **67**, 1727–1730 (1991).
14. S. L. Mielke, G. T. Foster, and L. A. Orozco, "Nonclassical intensity correlations in cavity QED," Phys. Rev. Lett. **80**, 3948–3951 (1998).
15. G. T. Foster, S. L. Mielke, and L. A. Orozco, "Intensity correlations in cavity QED," Phys. Rev. A **61**, 053821 (2000).
16. J. P. Clemens and P. R. Rice, "Nonclassical effects of a driven atoms-cavity system in the presence of an arbitrary driving field and dephasing," Phys. Rev. A **61**, 063810 (2000).
17. H. J. Carmichael, R. J. Brecha, and P. R. Rice, "Quantum interference and collapse of the wavefunction in cavity QED," Opt. Commun. **82**, 73–79 (1991).
18. R. J. Brecha, P. R. Rice, and M. Xiao, "*N* two-level atoms in a driven optical cavity: quantum dynamics of forward photon scattering for weak incident fields," Phys. Rev. A **59**, 2392–2417 (1999).
19. H. A. Bachor, *A Guide to Experiments in Quantum Optics* (Wiley, New York, 1998).
20. E. T. Jaynes and F. W. Cummings, "Comparison of quantum and semiclassical radiation theories with application to the beam maser," Proc. IEEE **51**, 89 (1963).
21. H. J. Carmichael, *An Open Systems Approach to Quantum Optics*, Lecture, Notes in Physics, New Series (Springer-Verlag, Berlin, 1993); Monograph 18.
22. M. Lax, "Formal theory of quantum fluctuations from a driven state," Phys. Rev. **129**, 2342–2348 (1963).
23. M. Lax, "Quantum noise. X. Density-matrix treatment of field and population-difference fluctuations," Phys. Rev. **157**, 213–231 (1967).
24. M. B. Plenio and P. L. Knight, "The quantum-jump approach to dissipative dynamics in quantum optics," Rev. Mod. Phys. **70**, 101–144 (1998).
25. P. R. Rice and H. J. Carmichael, "Nonclassical effects in optical spectra," J. Opt. Soc. Am. B **5**, 1661–1668 (1988).
26. M. D. Reid and D. F. Walls, "Squeezing via optical bistability," Phys. Rev. A **32**, 396–401 (1985).
27. H. M. Wiseman and G. J. Milburn, "Quantum theory of optical feedback via homodyne detection," Phys. Rev. Lett. **70**, 548–551 (1993).
28. A. C. Doherty, S. Habib, K. Jacobs, H. Mabuchi, and S. M. Tan, "Quantum feedback control and classical control theory," Phys. Rev. A **62**, 012105 (2000).